

Illumination Variation Correction Using Image Synthesis For Unsupervised Domain Adaptive Person Re-Identification

Jiaqi Guo

*School of Electrical and Computer Engineering, Purdue University
West Lafayette, IN, USA
guo498@purdue.edu*

Amy R. Reibman

*School of Electrical and Computer Engineering, Purdue University
West Lafayette, IN, USA*

Edward J. Delp

*School of Electrical and Computer Engineering, Purdue University
West Lafayette, IN, USA*

Abstract—Unsupervised domain adaptive (UDA) person re-identification (re-ID) aims to learn identity information from labeled images in source domains and apply it to unlabeled images in a target domain. One major issue with many unsupervised re-identification methods is that they do not perform well relative to large domain variations such as illumination, viewpoint, and occlusions. In this paper, we propose a Synthesis Model Bank (SMB) to deal with illumination variation in unsupervised person re-ID. The proposed SMB consists of several convolutional neural networks (CNN) for feature extraction and Mahalanobis matrices for distance metrics. They are trained using synthetic data with different illumination conditions such that their synergistic effect makes the SMB robust against illumination variation. To better quantify the illumination intensity and improve the quality of synthetic images, we introduce a new 3D virtual-human dataset for GAN-based image synthesis. From our experiments, the proposed SMB outperforms other synthesis methods on several re-ID benchmarks.

Index Terms—Person Re-ID, Unsupervised Domain Adaptation, Image Synthesis, Illumination Variation

I. INTRODUCTION

Given a person-of-interest (query image), the goal of person re-identification (re-ID) is to retrieve the images from a dataset of the same person-of-interest across different cameras at different times and locations (gallery images). The person re-ID problem is critical as it has wide applications in surveillance and security [42]. It is also challenging due to viewpoint and illumination variations across cameras, as well as potential occlusions, detection errors, and background clutter in query and gallery images [17]. With the recent advancement in deep neural networks (DNN), the person re-ID community has achieved very good progress relative to several re-ID benchmarks [31], [33], [38], [45]. In this paper, “domain” shall refer to a set of images with similar style (e.g., same illumination, viewpoint, cameras). We will also use the term

This material is based on research sponsored by U.S. Department of Homeland Security (DHS) under Grant Award Number 17STCIN0001. The U.S. Government is authorized to reproduce and distribute reprints for Governmental purposes notwithstanding any copyright notation thereon. The views and conclusions contained herein are those of the authors and should not be interpreted as necessarily representing the official policies or endorsements, either expressed or implied, of DHS or the U.S. Government.

“dataset” to indicates images from a domain. Most of the above studies were carried out under the supervised settings, where data from the same domain are split into training and test sets. However, when the trained DNN models are tested on new domains, there is usually a drastic performance degradation.

Re-ID data collection and annotation is expensive and labor intensive, which makes supervised methods less desirable. Therefore, unsupervised domain adaptive (UDA) person re-ID has attracted more and more attention over the past few years [2], [7], [27], [36], [49]. In the unsupervised scenario, we have access to one or more labeled domains (the “source domains”), and unlabeled images from another domain that we wish to use. We shall call this new domain the “target domain”. The goal is to improve the re-ID performance on the target domain.

One approach to UDA person re-ID problems is through image synthesis [3], [7], [36], [49]. Using labeled data from the source domains, most synthesis methods employed generative adversarial networks (GAN) to create labeled synthetic images that approximate the target domain. The synthetic images are used to fine tune pre-trained models from the source domains and then use the fine-tuned models on the target domain. Although the synthesis methods are effective, most of them mainly use single source domain [7], [36], [49], or a subset of a source domain with single illumination condition [3]. Few have considered the integration of multiple source domains or multiple illumination conditions. This potentially limits the performance of the fine-tuned re-ID models.

In this paper, we propose a Synthesis Model Bank (SMB) to deal with illumination variation. The basic idea of SMB is to use multiple (or a bank of) re-ID models. Each re-ID model is trained using synthetic images which have one of the most common illumination conditions in the target domain. Given one query image and one gallery image for that query, we select and use the most suitable model based on the illumination conditions of the query image and the gallery image. We assume that there are N different illumination conditions in the target domain. Our proposed model consists

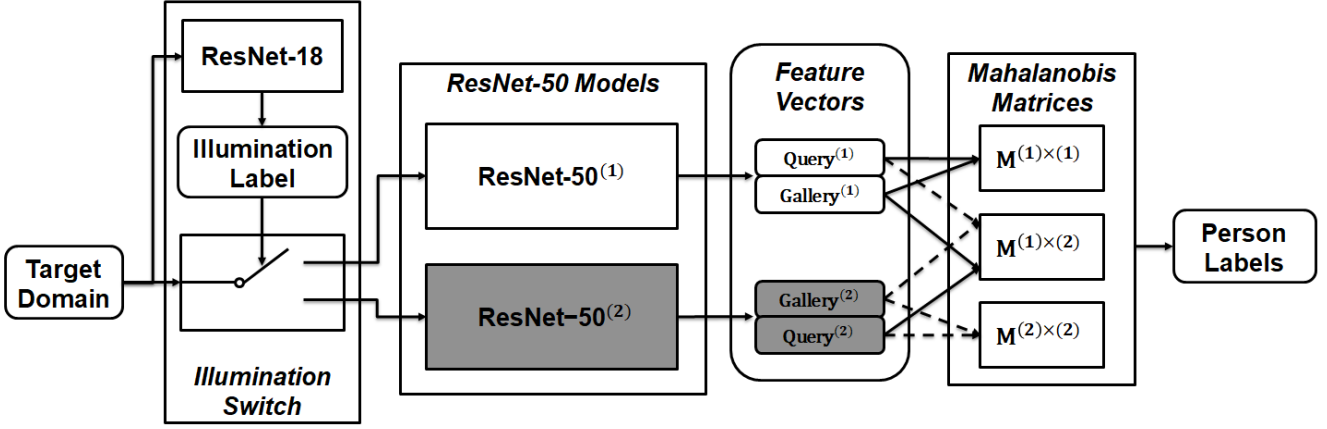


Fig. 1. Block diagram of the proposed **Synthesis Model Bank (SMB)** where we assume there are two illumination conditions in the target domain ($N = 2$).

of three components as shown in Figure I: 1) an Illumination Switch that uses ResNet-18 [14] to classify the query image and the gallery image into one of N illumination conditions. 2) N ResNet-50 [14] models that convert the query and the gallery images into feature vectors. Each ResNet-50 model is trained for a specific illumination condition. 3) $\frac{N \times (N-1)}{2} + N$ Mahalanobis Matrices that compute the distances between query and gallery feature vectors. Each Mahalanobis Matrix is used for a specific combination of query and gallery illumination conditions. When a query image and a gallery image are given as input, the Illumination Switch first estimates their illumination conditions. Based on the estimated illumination conditions of the query image and the gallery image, we select the corresponding ResNet-50 model and Mahalanobis Matrix to convert the input images into feature vectors and compute their distances for person identity retrieval.

The CNN models and the Mahalanobis Matrices in the Synthesis Model Bank are trained using the labeled synthetic images that approximate the target domain. The synthetic images have different illumination conditions. To generate the synthetic images, we extend the method in [3] into three major steps: 1) estimate the illumination conditions in the target domain; 2) select the first N source domains that have similar illumination conditions as the target domain; 3) use CycleGAN [50] to convert the selected source domains into N sets of labeled synthetic images. In [3], the source domains are 3D virtual-human images created using Unreal Engine 4 (UE4) [8], where the illumination conditions are indirectly controlled by environmental maps. In this paper, to better quantify the illumination intensity of target domain and to improve the quality of CycleGAN synthesis, we introduce the **Unreal Labeled Images for Person Re-Identification (ULI-RI)**, a new 3D virtual-human dataset that have images labeled by illumination intensity, as well as person identity, model z-rotation angle, and background. The ULI-RI is created using Unreal Engine 4 (UE4) to simulate various outdoor environments with 115 high-quality 3D human models. The illumination in the ULI-RI is directly controlled using the

SunSky asset such that the illumination labels is linked to the illumination intensity.

Our major contributions in this paper can be summarized as follows:

- We introduce a new 3D virtual-human dataset for person re-ID which have images labeled by illumination intensity as well as person identity, model rotation angle, and background.
- We propose a Synthesis Model Bank (SMB) to deal with illumination variation in the target domain for unsupervised person re-ID.
- Our experiments show that the proposed SMB outperforms other synthesis methods on several re-ID benchmarks.

II. RELATED WORK

A. Deep Neural Networks for Person Re-ID

With the recent advancement in deep neural networks (DNN), the person re-ID performance has achieved very good progress on several benchmark tests [31], [33], [38], [45]. A re-ID system based on deep neural networks typically include the feature extraction learning [42], which aims to learn deep feature embeddings/vectors from input images. Since deep neural networks are initially designed for image classification problems [5], [14], [19], [32], many deep re-ID networks follow the classification framework and view the training procedures of person re-ID as a classification problem, where each person (identity) in the dataset is treated as a unique class. Usually an extra fully connected layer with Batch Normalization is added before the CrossEntropy layer to define the feature vectors [30], [31], [41], [48]. In this paper, we follow the practice in [3] and use ResNet-50 [14] for feature vector extraction in our proposed Synthesis Model Bank.

B. Synthesis Methods for Unsupervised Domain Adaptive Person Re-ID

Since generative adversarial networks (GANs) [11] were first described, using synthetic data for fine-tuning deep neural

TABLE I
3D VIRTUAL-HUMAN DATASETS USED FOR PERSON RE-ID

Name	Software	Identity	Background (Camera)	Viewpoint (Model Z-Rotation)	Illumination	Bounding Box
SOMAset	Blender	50		8 clothing sets and 250 poses for each identity		100'000
PersonX	Unity	1266	6	36	-	273'456
GPR+	GTA5	808	- (random)	12	7 (daytime) \times 7 (weather)	475'104
SyRI	UE4	100		4 (fix models, rotate cameras)	140	56'000
ULI-RI	UE4	115	8	8	8	58'880

networks has drawn more and more attention. An import direction to improve person re-ID performance in unsupervised settings is through synthesis data augmentation. GANs are used to learn the style of the target domain, and transfer the style to source domains to create labeled synthetic images. In [7], the authors proposed SPGAN which captures self-similarity and domain dissimilarity to preserve images quality after GAN translation. In [36], Wei et al. explored semantic segmentation map to introduce an extra regularization term in loss function and proposed PTGAN. In [49], Zhong et al. explored a camera-specific strategy to transfer one source domain to every sub-target domain. In [3], Bak et al. proposed a method which first selects the subset of a virtual-human dataset according to the illumination in the target domain, and then use CycleGAN to generate synthetic images from the selected subset. The method in [3] achieved the best performance relative to other synthesis methods on several benchmark datasets. The subset-selection has proved to be effective on closing the gap between the distributions of the synthetic images and the target domain. However, the method in [3] assumed there was only one illumination condition in each target domain, whereas images collected from real-life surveillance cameras often have more complicated illumination conditions.

C. 3D Virtual-Human Datasets

Three dimensional virtual-human images are generally created using a game engine with 3D human models such as described in [3], [29] or from screenshots of human characters taken from a video game such as in [39]. In this paper, the virtual-human images are used as input to CycleGAN [50] to generate the synthetic images for training the proposed Synthesis Model Bank. We summarize the existing 3D virtual-human datasets for person re-ID in Table I. SOMAset [4] contains 50 identities and is used for the re-ID when the same person has different clothing and accessories. PersonX [29] is specially designed to study the effects of viewpoint variation. Both SOMAset and PersonX do not include illumination variation when generating the images. GPR+ [39] is a large-scale virtual-human dataset with rich diversity. The authors controlled the daytime and weather in a video game to obtain various illumination conditions. SyRI [3] uses 140 High Dynamic Range (HDR) environment maps that were acquired from indoor and outdoor panoramas as background and light sources to render the UE4 gaming engine scenes. Although the authors in [3] claim that images from the same HDR map have the same illumination condition, the relative positioning

between the UE4 virtual camera and the light sources in the environment causes noticeable illumination variation even for images in the same HDR map. The illumination conditions in GPR+ and SyRI are indirectly controlled through daytime, weather, or environment maps. It is difficult to understand the relative illumination intensity from the “illumination labels” in GPR+ and SyRI.

III. OUR PROPOSED APPROACH

A. Problem Description and Annotation

In this paper, “real” refers to images collected by actual surveillance cameras in the real world, and “virtual” refers to the images generated using a gaming engine such as the Unreal Engine 4 (UE4) [8], and “synthetic” refers to the images generated using GANs such as CycleGAN [11], [50]. In unsupervised domain adaptive person re-ID, we have access to one or several labeled source domains, and aim to achieve better re-ID performance on a real, unlabeled target domain. The source domains can be either real or virtual.

We denote the set of M real source domains as $\mathbf{R} = \{\mathbb{R}_1, \mathbb{R}_2, \dots, \mathbb{R}_M\}$, where $\mathbb{R}_m = \{(r_i, y_i)\}_{i=1}^{|\mathbb{R}_m|}$ ($m \in \{1, 2, \dots, M\}$) is a real-life re-ID dataset with $|\mathbb{R}_k|$ images (r_i) and their identity labels (y_i). We denote the set of N virtual source domains as $\mathbf{V} = \{\mathbb{V}_1, \mathbb{V}_2, \dots, \mathbb{V}_N\}$, where $\mathbb{V}_n = \{(v_i, y_i)\}_{i=1}^{|\mathbb{V}_n|}$ ($n \in \{1, 2, \dots, N\}$) is a virtual (game engine generated) re-ID dataset with $|\mathbb{V}_n|$ images (v_i) and their identity labels (y_i). In some virtual source domains, image v_i also has labels for illumination (u_i). We denote the set of N synthetic domains (GAN generated) as $\mathbf{S} = \{\mathbb{S}_1, \mathbb{S}_2, \dots, \mathbb{S}_N\}$. In this paper, we assume the synthetic domain \mathbb{S}_n is generated from the corresponding virtual source domain \mathbb{V}_n using GAN based methods and not generated from the real world images. Finally, we denote the real world target domain as $\mathbf{T} = \{(t_i, y_i)\}_{i=1}^{|\mathbb{T}|}$, with $|\mathbb{T}|$ images (t_i) and their identity labels (y_i). The identity labels in the target domain are used only for testing.

B. Generating Synthetic Images for Training

To train the proposed Synthesis Model Bank (SMB), we first need to generate the synthetic images according to the most common illumination conditions in the target domain. We extend the GAN approach in [3] for generating the synthetic images. As illustrated in Figure 2, the extended approach can be summarized into three steps: 1) estimate the N most common illumination labels in the target domain using an Illumination Inference model; 2) according to the estimated illumination labels, select N subsets from the virtual-human

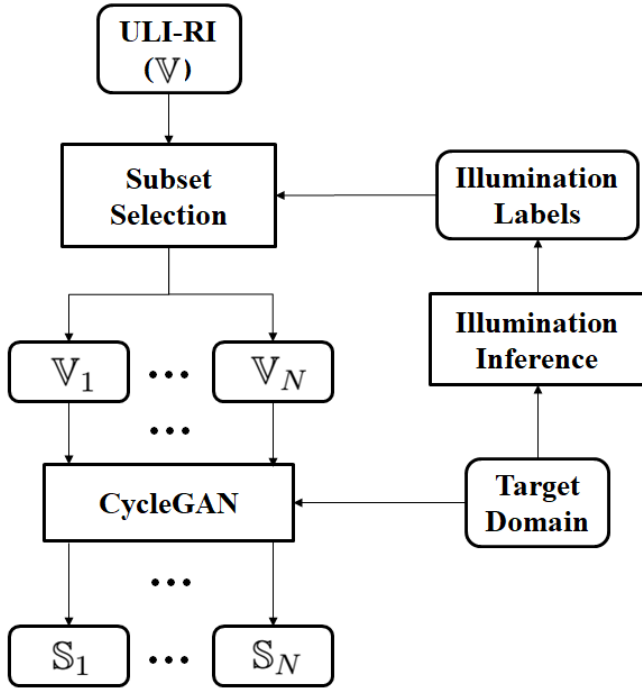


Fig. 2. Generating synthetic images using our proposed virtual-human dataset, ULI-RI (detailed descriptions can be found in Section IV-A). The selected subsets are used as N virtual source domains (\mathbb{V}_n for $n \in \{1, 2, \dots, N\}$); 3) use CycleGAN [50] to convert each selected source domain \mathbb{V}_n into a set of synthetic images \mathbb{S}_n . The synthetic images in \mathbb{S}_n have the same illumination condition as \mathbb{V}_n , and also approximate the style of the target domain.

dataset, ULI-RI (detailed descriptions can be found in Section IV-A). The selected subsets are used as N virtual source domains (\mathbb{V}_n for $n \in \{1, 2, \dots, N\}$); 3) use CycleGAN [50] to convert each selected source domain \mathbb{V}_n into a set of synthetic images \mathbb{S}_n . The synthetic images in \mathbb{S}_n have the same illumination condition as \mathbb{V}_n , and also approximate the style of the target domain.

1) *Illumination Inference and Subset Selection:* The **Illumination Inference** in Figure 2 is a ResNet-18 classifier [14] which is trained using the 3D human images in the ULI-RI dataset and their illumination labels as 8 classes. The **Illumination Inference** is used to estimate the illumination labels of the target domain: $\mathbf{II} : \mathbb{T} \rightarrow \{1, 2, \dots, 8\}$. The most common illumination label n^* in the target domain is defined as:

$$n^* = \arg \max_{n \in \{1, 2, \dots, 8\}} \sum_{i=1}^{|\mathbb{T}|} \mathbb{1}(\mathbf{II}(t_i) == n), \quad (1)$$

where $\mathbb{1}(\cdot)$ is the indicator function, t_i is the image in the target domain \mathbb{T} . Next, the subset of ULI-RI that have illumination label n^* is selected to be the first virtual source domain, \mathbb{V}_1 . Similarly, we create the virtual source domains $\mathbb{V}_2, \dots, \mathbb{V}_N$ according to the rest $N - 1$ most common illumination labels of the target domain.

From our experiments, most of the images in a target domain (over 80%) have the top two most common illumination labels. Therefore, we set $N = 2$ in this paper, i.e.,



Fig. 3. Generating synthetic images for the target domain PRID dataset [15]. Top: images in the target domain ($t_i \in \mathbb{T}$). Middle: images in the selected subsets of ULI-RI, i.e., the two virtual source domains \mathbb{V}_1 (left) and \mathbb{V}_2 (right). Bottom: synthetic images generated using the virtual source domains, i.e., \mathbb{S}_1 (left) and \mathbb{S}_2 (right). The target domain images on the left and those on the right have different illumination conditions.

we assume there are two major illumination conditions in a target domain. According to the top two illumination labels, we create two virtual source domains \mathbb{V}_1 and \mathbb{V}_2 , which will be used independently for generating synthetic images using CycleGAN [50].

2) *Using CycleGAN to Generate Synthetic Images:* Given the images from a virtual source domain $v_i \in \mathbb{V}$ and the images from the target domain $t_i \in \mathbb{T}$, CycleGAN learns two translation functions $G : \mathbb{V} \rightarrow \mathbb{T}$ and $F : \mathbb{T} \rightarrow \mathbb{V}$ that can transfer the styles between the two domains [50]. In this paper, the translation function $G : \mathbb{V} \rightarrow \mathbb{T}$, which transfers the images in the virtual source domains to the target domain, is needed for generating the synthetic images. The transferred images, i.e. $G(\mathbb{V})$, are denoted as the synthetic images. Two adversarial networks $D_{\mathbb{V}}$ and $D_{\mathbb{T}}$ acting as discriminators are trained along with G and F . $D_{\mathbb{V}}$ aims to discriminate the images in the virtual source domain from images generated by F . Analogously, $D_{\mathbb{T}}$ aims to discriminate the images in the target domain from images generated by G .

The CycleGAN loss for training the networks is defined as

$$\begin{aligned} & \mathcal{L}(G, F, D_{\mathbb{V}}, D_{\mathbb{T}}) \\ &= \mathcal{L}_{GAN}(G, D_{\mathbb{T}}, \mathbb{V}, \mathbb{T}) + \mathcal{L}_{GAN}(F, D_{\mathbb{V}}, \mathbb{V}, \mathbb{T}) \\ & \quad + \lambda_1 \mathcal{L}_{cycle}(G, F) + \lambda_2 \mathcal{L}_{id}(G, F) + \lambda_3 \mathcal{L}_{Mask}(G) \end{aligned} \quad (2)$$

with three parameters (λ_1, λ_2 , and λ_3) controlling the weights of each term. As defined in the original paper [50], $\mathcal{L}_{GAN}(G, D_{\mathbb{T}}, \mathbb{V}, \mathbb{T})$ and $\mathcal{L}_{GAN}(F, D_{\mathbb{V}}, \mathbb{V}, \mathbb{T})$ are the adversarial loss, $\mathcal{L}_{cycle}(G, F)$ is the cycle consistency loss to avoid the problem of mode collapse (same output for all input) [3], $\mathcal{L}_{id}(G, F)$ is the identity loss which restricts the semantic shift of the translation functions G and F , and $\mathcal{L}_{Mask}(G)$ is adapted

from the reference loss [3], [26] to make sure that the synthetic images keep the identity features from the virtual images.

For a specific target domain \mathbb{T} , the two virtual source domains selected as in Section III-B1 (\mathbb{V}_1 and \mathbb{V}_2) are used independently for generating two synthetic domains \mathbb{S}_1 and \mathbb{S}_2 . Figure 3 shows the example synthetic images when using the PRID dataset [15] as target domain. As shown in Figure 3, there are two major illumination conditions in the PRID dataset. Using the Illumination Inference and CycleGAN, we generate two synthetic domains according to these illumination conditions. The generated synthetic images inherit the illumination conditions and the identity labels of the virtual source domains, and also have similar styles as the target domain.

C. Synthesis Model Bank

The basic concept of the proposed Synthesis Model Bank (SMB) for re-ID is to train multiple (or a bank of) re-ID models, and use the most suitable models according to the illumination conditions of the query image and the gallery image. As shown in Figure I, the proposed SMB consists of three components: 1) an Illumination Switch that uses ResNet-18 [14] to classify the query image and the gallery image into one of N illumination conditions. 2) N ResNet-50 [14] models that convert the query and the gallery images into feature vectors. Each ResNet-50 model is trained for a specific illumination condition. 3) $\frac{N \times (N-1)}{2} + N$ Mahalanobis Matrices that compute the distances between query and gallery feature vectors. Each Mahalanobis Matrix is used for a specific combination of query and gallery illumination conditions.

As discussed in Section III-B1, we assume $N = 2$, i.e., there are two major illumination conditions in each target domain. When a query image and a gallery image are given as input, the Illumination Switch first estimates their illumination conditions. Based on the estimated illumination conditions of the query image and the gallery image, we select the corresponding ResNet-50 model and Mahalanobis Matrix to convert the input images into feature vectors and compute their distances for person identity retrieval.

1) **Illumination Switch:** The **Illumination Switch** in the SMB is used to estimate the illumination conditions of the input images. Since we assume each image in the target domain have one of the two most common illumination conditions, the **Illumination Switch** is trained to classify the input images into one of these two illumination conditions.

Similar to the Illumination Inference in Section III-B1, we use ResNet-18 [14] in the **Illumination Switch** to train a binary classifier. The images from the generated synthetic domains \mathbb{S}_1 and \mathbb{S}_2 are used as training data. The images in \mathbb{S}_1 are labeled as “ l_1 ” and the images in \mathbb{S}_2 are labeled as “ l_2 ”.

2) **Feature Vectors:** After estimating the illumination conditions using the **Illumination Switch**, the query image and the gallery image are assigned to the corresponding ResNet-50 models to be converted into feature vectors. As shown in Figure I, when $N = 2$, images which are labeled as “ l_1 ” are assigned to ResNet-50⁽¹⁾, and analogously, images which are labeled as “ l_2 ” are assigned to ResNet-50⁽²⁾.

Each model uses a ResNet-50 [14] and is trained as a classification problem (identities as classes) [47]. Following the practice in [30], [49], we added two fully connected layers before the CrossEntropy layer to improve the training accuracy. The output of the first fully connected layer is 1024 dimensional and is followed by Batch-Normalization [16], ReLU, and Dropout [28]. The second fully connected layer is $1024 \times N_S$, where N_S is the number of identities in the training set. After the models are trained, we use the output of the first fully connected layer as the feature vectors.

We pre-train a baseline model using a combination of both real and virtual source domains (CUHK03 [21], DukeMTMC4ReID [24], and SyRI [3]). This combined domain consists of a significantly large number of identities (more than 3K) to represent the general identity features. To adapt to a specific illumination condition in the target domain, each ResNet-50 model is fine tuned from this baseline model using the corresponding synthetic domain. When $N = 2$, \mathbb{S}_1 and \mathbb{S}_2 are used to fine tune ResNet-50⁽¹⁾ and ResNet-50⁽²⁾ respectively.

3) *Mahalanobis Matrices:* The query image and the gallery image from the target domain are first classified by the Illumination Switch, and then assigned to the corresponding ResNet-50 models to be converted into feature vectors. The last step is to compute the distance between the query and the gallery feature vectors for identity retrieval. Since the feature vectors from different CNN models might be different in scale, we propose to learn several Mahalanobis Matrices to address this problem. To learn a Mahalanobis Matrix is to learn a global, linear transformation of the feature vectors [18], and the goal is to emphasize the relevant dimensions and diminish the irrelevant ones in the new feature space. For a set of feature vectors and their labels ($\{(\mathbf{x}_i, y_i)\}_{i=1}^K$), a Mahalanobis Matrix, \mathbf{M} , computes the squared distance between two vectors \mathbf{x}_i and \mathbf{x}_j as:

$$d_{\mathbf{M}}^2(\mathbf{x}_i, \mathbf{x}_j) = (\mathbf{x}_i - \mathbf{x}_j)^T \mathbf{M} (\mathbf{x}_i - \mathbf{x}_j) \quad (3)$$

and an algorithm to learn the Mahalanobis Matrix aims to minimize the distances within the same class while maximize the distance between different classes. As shown in Figure I, when $N = 2$, we need three Mahalanobis Matrices for different illumination conditions: 1) Mahalanobis Matrix $\mathbf{M}^{(1) \times (1)}$ is used when both feature vectors have illumination condition l_1 . 2) Mahalanobis Matrix $\mathbf{M}^{(2) \times (2)}$ is used when both feature vectors have illumination condition l_2 . 3) Mahalanobis Matrix $\mathbf{M}^{(1) \times (2)}$ is used when query and gallery feature vectors have different illumination conditions.

There are several methods to find the Mahalanobis Matrix for a dataset through defining and optimizing an objective function [6], [13], [18], [37]. We choose the **Keep It Simple and Straightforward MEtric (KISSME)** [18] for its broad applicability on various benchmarks including some for person re-ID. For the first two cases where the target domain feature vectors have the same illumination, we can directly train $\mathbf{M}^{(1) \times (1)}/\mathbf{M}^{(2) \times (2)}$ using all pairs of feature vectors from $\mathbb{S}_1/\mathbb{S}_2$. For the third case where the target domain feature

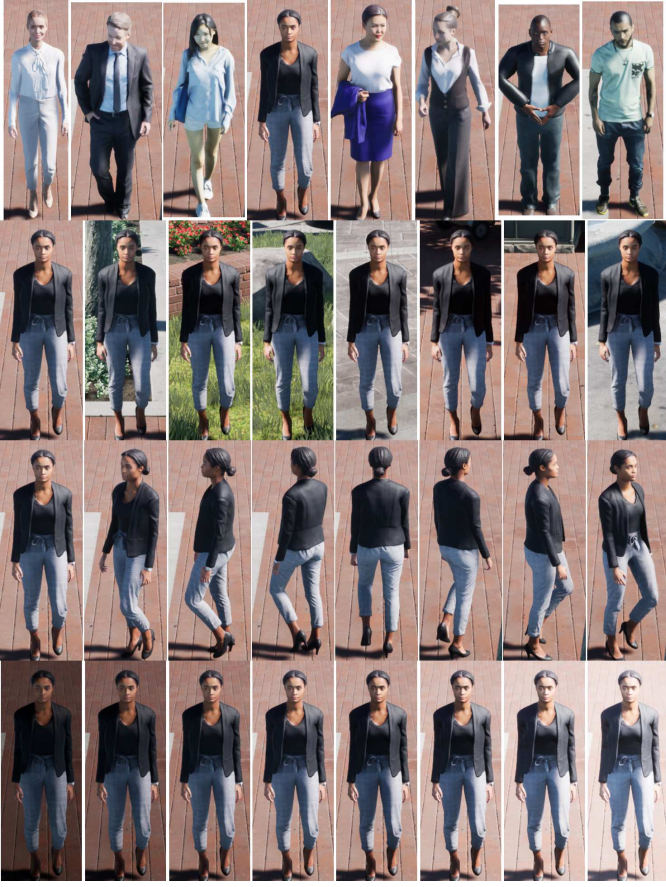


Fig. 4. Example images from the ULI-RI dataset First row: 8 different identities in the ULI-RI Second row: the same identity with 8 different backgrounds (cameras) Third row: the same identity with 8 different model z-rotation angle (viewpoints) Fourth row: the same identity under 8 different illumination conditions

vectors have different illuminations, the pairs of feature vectors for training $M^{(1) \times (2)}$ should also have different illumination conditions.

IV. EXPERIMENTS AND EVALUATION

A. ULI-RI Dataset (Virtual Source Domain)

The virtual source domains in this paper are 3D virtual-human images generated using the Unreal Engine 4 (UE4) [8]. They are the inputs to CycleGAN to generate the synthetic images for training the Synthesis Model Bank. To better quantify the illumination intensity in the target domain and improve the quality of CycleGAN synthesis, we introduce the Unreal Labeled Images for Person Re-Identification (ULI-RI), a new 3D virtual-human dataset for person re-ID. The images in the ULI-RI dataset are labeled by illumination intensity as well as person identity, model z-rotation angle, and background. The ULI-RI dataset is generated using UE4 to simulate various outdoor environments with 115 high-quality 3D human models. The illumination in the ULI-RI is directly controlled using the **SunSky** asset of UE4 such that

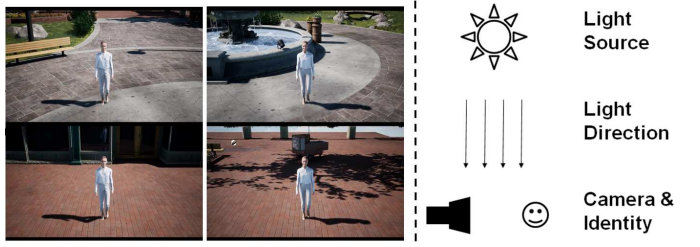


Fig. 5. Illustration of the camera setup in the virtual environment. Left: example images of the selected locations; Right: relative camera-light source locations

the illumination labels are linked to the illumination intensity. Example images from the ULI-RI are shown in Figure 4.

Camera and Background: We use the *Downtown West Modular Pack* [1] to setup the virtual environment. This simulates a large outdoor shopping mall and its surrounding areas, with hundreds of high quality models of buildings, gardens, decorations and other construction pieces. We select 8 locations (examples shown in Figure 5 Left) in the environment to set up virtual surveillance cameras such that 1) the images have less shadows 2) the camera facing direction is vertical to the light direction (as shown in Figure 5 Right); 3) the backgrounds are different. The first two points make sure that under the same UE4 light settings, the person in different images have similar illumination conditions. The third point makes sure that there are diverse backgrounds in the ULI-RI dataset.

Model Z-Rotation Angle (Viewpoint): The viewpoint refers to the angle between the person facing direction and the virtual camera facing direction. In UE4, this is controlled by the human model z-rotation angle. For every background and illumination condition, we set 8 values for model z-rotation angle ranging from 0° to 315° in step of 45° . We assign z-rotation label “0” to the images where the person is facing the camera, and the rest of the z-rotation labels are assigned in sequence as the person rotates clockwise along its z-axis. The third row in Figure 4 gives an example of the same identity at 8 different model z-rotation angles (background and illumination fixed), and from left to right their z-rotation labels are 0 to 7.

Illumination Condition: We use the SunSky asset in UE4 to achieve a direct link between the illumination labels and the illumination intensities. We set the SunSky asset as the only light source in the UE4 virtual environment. The illumination intensity is adjusted through the **light intensity parameter** of “DirectionalLight” component of the SunSky asset. We use an adjusted exponential function to map the illumination label to the light intensity parameter since it mostly follows the Weber’s law [25] and shows linear changes from human perceptions. Mathematically, given an illumination label $I \in \{0, 1, \dots, 7\}$, the **light intensity parameter** of SunSky (L) is set by

$$L = \exp(I \times 0.5 + 0.6) - 1 ;$$

The last row of Figure 4 gives an example of the same identity

with 8 different illumination labels (background and z-rotation fixed). From left to right their illumination labels are 0 to 7.

3D Human Models: There are 115 3D human models (identities) in the ULI-RI dataset, which are selected to cover a wide range of gender, race, age, clothing, and accessories. Most of the models are collected from online resources such as UE Marketplace. When taking the photos, the 3D human models are placed at the center of the camera view, and we rotate the models along their z-axis to get different viewpoints. Every time the illumination intensity, background (camera), or model z-rotation angle is changed, we re-rendered the entire environment to generate more realistic 3D human images. In conclusion, we create a total of 115 (identity) \times 8 (background) \times 8 (z-rotation) \times 8 (illumination condition) = 58,880 images, 512 for each identity.

B. Re-ID Benchmark Datasets (Target Domain)

In the unsupervised re-ID scenario, we have access to one or more labeled domains (the “source domains”), and unlabeled images from another domain that we wish to use. This new domain is known as the “target domain”. In this paper, the experiments use 5 publicly available benchmark datasets as the target domains: PRID2011 [15], iLIDS-VID [35], Market-1501 [46], CUHK01 [20], and VIPeR [12]. We follow the testing protocols in [22], [40] for splitting the target domains into query and gallery sets (details can be found below). The re-ID performance of SMB for each target domain is evaluated and reported using rank-1 Cumulative Matching Characteristics (CMC-1) accuracy [12].

PRID2011 contains images captured from two static surveillance cameras. Camera A captured 385 identities, and Camera B captured 749 identities. We follow the single-shot settings and keep only one image for each identity from each camera. There are 200 identities that appeared in both cameras. For each experiment, half (100) of the 200 identities who appeared in both cameras are randomly chosen. Their images from Camera A are used as the query set, and their images from Camera B along with the images of the rest 549 identities are used as the gallery set. There are 100/649 images in the query/gallery sets.

VIPeR contains 632 identities taken by two cameras with illumination and viewpoint variations. Each identity has one image from camera_a and one image from camera_b. For each experiment, half (316) of the 632 identities are randomly chosen. The images from camera_a are used as query set and the images from camera_b as gallery set. There are 316/316 images in the query/gallery sets.

CUHK01 contains 971 identities in a campus environment that are captured by two surveillance cameras. There are two images for each identity in each camera, and a total of 3884 images in the dataset. For each experiment, 486 identities are randomly chosen. For each of the 486 identities, one random image from the first camera is used as the query image and

TABLE II
CMC-1 ACCURACY OF THE SYNTHESIS MODEL BANK AND THE SINGLE-ILLUMINATION MODELS ON DIFFERENT TARGET DOMAINS

Target Domain	Baseline	\mathbb{S}_1	\mathbb{S}_2	SMB
PRID2011	21.0	43.0	44.0	46.0
VIPeR	38.3	46.1	45.4	48.2
CUHK01	50.8	57.1	56.1	57.8
iLIDS-VID	21.7	36.2	35.8	36.3
Market-1501	58.4	65.3	64.3	66.8

\mathbb{S}_1 : The single-illumination model corresponds to the first illumination condition; \mathbb{S}_2 : The single-illumination model corresponds to the second illumination condition; SMB is the proposed Synthesis Model Bank.

one random image from the second camera as the gallery image. There are 486/486 images in the query/gallery sets.

iLIDS-VID contains 300 identities captured by two cameras. Each identity has one image from each camera (600 images in total). For each experiment, we randomly select 150 identities, and their images from camera 01/02 are used as the query/gallery set. There are 150/150 images in the query/gallery sets.

Market-1501 contains 1501 identities and 32668 images from 6 cameras. The Market-1501 dataset is already split into two parts by the authors [46]: the first 751 identities and their 12936 images is used as the training set and the other 750 identities and their 19732 images as the testing set. The testing set is further split into the query and the gallery sets following the protocols in [43], [46]. There are 3368/19732 images in the query/gallery sets.

C. Single-Illumination Model versus Synthesis Model Bank

To demonstrate the effectiveness of using multiple illumination conditions, we compare the Synthesis Model Bank to the single-illumination model. Each single-illumination model consists of one ResNet-50 and the corresponding Mahalanobis Matrix as shown in Figure I. The single-illumination models can be seen as a simplified version of the Synthesis Model Bank where we assume only one illumination condition in the target domain. The Illumination Switch and the Mahalanobis Matrix for different illumination inputs (e.g., $\mathbf{M}^{(1) \times (2)}$ in Figure I) are always omitted in the single-illumination models.

For each target domain, there are two single-illumination models (denoted as \mathbb{S}_1 and \mathbb{S}_2) corresponding to the two most common illumination conditions. In the experiments, we split the target domain into query and gallery sets as described in Section IV-B. The Synthesis Model Bank and the single-illumination models are tested independently on the target domains to retrieve the identities in the query set from the gallery set. The experiment results are reported using CMC-1 accuracy [12] in Table II. We also include the results of the pre-trained baseline model (ResNet-50 before fine-tuning) described in Section III-C2 as reference. From Table II, the two single-illumination models of each target domain both improve the re-ID accuracy compared with the baseline model. The two single-illumination models also have similar

TABLE III

SINGLE-ILLUMINATION MODEL TESTED WITH THE CORRESPONDING SINGLE ILLUMINATION INPUT

Target Domain	Illumination Condition	Query Image	Gallery Image	Valid Query	CMC-1 Accuracy
PRID2011	(1)	51	343	27	59.3
	(2)	49	306	24	54.2
VIPeR	(1)	149	171	97	51.6
	(2)	167	145	93	55.7
CUHK01	(1)	400	408	345	71.6
	(2)	86	78	23	78.3
iLIDS-VID	(1)	100	103	67	44.8
	(2)	50	47	15	46.7
Market-1501	(1)	2088	11344	2036	76.1
	(2)	1280	8388	1218	73.6

performance on most target domains, possibly due to the fact that the numbers of images in the two illumination conditions are close. Compared with the single-illumination models, the Synthesis Model Bank further improves the re-ID performance through integrating both illumination conditions.

D. Single-Illumination Model with the Corresponding Single Illumination Input

To understand how the single-illumination models perform within the Synthesis Model Bank, we test the single-illumination models when the input images have the “correct” illumination condition. The original query and gallery sets are each split into 2 subsets according to the illumination conditions of the images. This generates four subsets for a target domain: Query⁽¹⁾, Query⁽²⁾, Gallery⁽¹⁾, and Gallery⁽²⁾ (superscript indicating the illumination condition). To test the performance of the first single-illumination model, we use the combination of Query⁽¹⁾ and Gallery⁽¹⁾ as target domain. Analogously, we use the combination of Query⁽²⁾ and Gallery⁽²⁾ to test the second model. In the original target domains, some query images have only one match in the gallery set, and sometimes the query image and its match have different illumination conditions. Therefore, when using the combination of Query⁽ⁿ⁾ and Gallery⁽ⁿ⁾ as target domain, we exclude the images in Query⁽ⁿ⁾ that do not have a match in Gallery⁽ⁿ⁾ ($n \in 1, 2$).

Table III summarizes the experimental results. Each target domain has two rows corresponding to the two single-illumination models. The number of query and gallery images in each test case are reported in the third and the fourth column. The fifth column gives the number of valid query images, i.e., the query images that have a match in the gallery set. Comparing the results in Table III to the results in Table II, the single-illumination models with the corresponding illumination input have better CMC-1 accuracy than the single-illumination models with the original target domain. This shows that the single-illumination models have the best performance within the correct illumination condition. The single-illumination models with the corresponding illumination input also have better performance compared to the Synthesis Model Bank with the original target domain (last column of Table

II). This gap of performance is mainly caused by directly comparing the distances from different Mahalanobis Matrices in the Synthesis Model Bank. For instance, a query image from Query⁽¹⁾ needs to be compared to the gallery images from both Gallery⁽¹⁾ and Gallery⁽²⁾ in the Synthesis Model Bank. In this case, the distances from $\mathbf{M}^{(1) \times (1)}$ and the distances from $\mathbf{M}^{(1) \times (2)}$ are compared directly, which causes some correct retrievals within $\mathbf{M}^{(1) \times (1)}$ being misled by $\mathbf{M}^{(1) \times (2)}$.

E. Comparison with Other Unsupervised Domain Adaption Methods for Person Re-ID

Here we compare the proposed Synthesis Model Bank with other unsupervised domain adaption (UDA) methods for person re-identification. While searching for related studies, we focus on unsupervised methods that carried out experiments on any of the target domains mentioned in Section IV-B. These UDA methods for person re-ID can be categorized into three types: 1) feature vector operation (FVO) [23], [34], [43] which uses CNN or hand-crafted methods to transfer feature vectors from different domains into a shared domain for comparing; 2) synthesis augmentation (SA) [3], [7], [36], [49] which generates synthetic images using GAN-based methods for fine tuning re-ID models; and 3) pseudo labeling (PL) [2], [9], [10], [44], [51] which iteratively uses clustering methods to generate pseudo labels for the target domain images and re-train re-ID models.

Table IV summarizes the results of the reviewed methods. Among all FVO and SA methods, the proposed Synthesis Model Bank achieves the best performance on most target domains. With the same source domains for training the baseline model, our method outperforms the method in [3] by 1.1-5.2% on various target domains. On the specific target domain, Market-1501, most recent pseudo-labeling methods outperforms the synthesis-augmentation methods even with limited source domain (CMC-1 accuracy on Market-1501: UMSDA [2]-94.8%, MMT [10]-88.4%, NRMT [9]-87.8%). Instead of indirectly learning information about the target domain through synthetic data, the pseudo-labeling methods directly use the target domain images during the iteratively training process. This indicates that there is still a gap between the distributions of the synthetic data and the target domain. The pseudo-labeling methods are not included in Table IV since most of them only used Market-1501 as target domain. Using the small-scale re-ID benchmark datasets as target domain is not reported in the pseudo-labeling methods.

V. CONCLUSION

In this paper, we introduced **Unreal Labeled Images for Person Re-Identification (ULI-RI)**, a new 3D virtual-human dataset for person re-ID to better quantify the illumination intensity and improve the quality of CycleGAN synthesis. The virtual dataset provides rich diversity and has images labeled by illumination intensity as well as person identity, model z-rotation angle, and background. In addition, we described the Synthesis Model Bank to address illumination variation. The Synthesis Model Bank makes use of synthetic data from

TABLE IV
COMPARISON WITH OTHER UNSUPERVISED DOMAIN ADAPTION METHODS FOR PERSON RE-ID

	Method	Source	PRID2011	ViPeR	CUHK01	iLIDS-VID	Market-1501
FVO	TL [23]	Mixed [23]	24.2	31.5	27.1	-	-
	TJ-AIDL [34]	Market	26.8	38.5	-	-	-
	TJ-AIDL [34]	Duke	34.8	35.1	-	-	58.2
	CAMEL [43]	JSTL [40]	-	30.9	57.3	-	54.5
SA	PTGAN [36]	Duke	-	-	-	-	38.6
	PTGAN [36]	CUHK03	37.5	-	-	-	-
	SyRI [3]	$R^a + S^b$	43.0	43.0	54.9	-	65.7
	SPGAN+LMP [7]	Duke	-	-	-	-	58.1
	CamStyle+LMP [49]	Duke	-	-	-	-	64.7
	Model Bank (Ours)	$R^a + S^b$	46.0	48.2	57.8	36.3	66.8

^a R is the real source domain which includes CUHK03 [21] and DukeMTMC4ReID [24]. ^b S is a virtual source domain SyRI [3].

“-” means the target domain is not tested in the original paper. All results are reported using the CMC-1 accuracy.

different illumination conditions to train multiple CNNs and Mahalanobis matrices. We then use the most suitable CNN and Mahalanobis matrix to find gallery images in target domain according to their illumination given a query image. From our experiments, the Synthesis Model Bank can effectively improve the performance of single-illumination models and outperform other synthesis methods by a large margin. In addition, from the experiments with specific illumination conditions, it is possible to further improve the Synthesis Model Bank through jointly learned Mahalanobis matrices.

There is a gap between synthesis methods (including the Synthesis Model Bank) and pseudo-label methods on the specific dataset Market-1501. This indicates the distribution of the synthetic data still differs from the actual domain. This gap could be closed by more advanced GANs techniques such as StyleGAN and BiCycleGAN, which will be studied in the future.

DECLARATION OF INTEREST

The authors declare that they have no conflict of interest.

REFERENCES

- [1] Downtown West modular pack in environments - UE marketplace. *Unreal Engine*, 2020.
- [2] Z. Bai, Z. Wang, J. Wang, D. Hu, and E. Ding. Unsupervised multi-source domain adaptation for person re-identification. *Computer Vision and Pattern Recognition (CVPR 2021 Oral)*, 2021.
- [3] S. Bak, P. Carr, and J.-F. Lalonde. Domain adaptation through synthesis for unsupervised person re-identification. *Proceedings of the European Conference on Computer Vision (ECCV)*, pages 189–205, 2018.
- [4] I. Barros Barbosa, M. Cristani, B. Caputo, A. Rognhaugen, and T. Theoharis. Looking beyond appearances: Synthetic training data for deep cnns in re-identification. *Computer Vision and Image Understanding*, 167:50–62, January 2017.
- [5] Y. Bengio and Y. LeCun. Large scale metric learning from equivalence constraints. *3rd International Conference on Learning Representations*, page 1409.1556, 2015.
- [6] J. V. Davis, B. Kulis, P. Jain, S. Sra, and I. S. Dhillon. Information-theoretic metric learning. *Proceedings of the 24th international conference on Machine learning*, pages 209–216, June 2007.
- [7] W. Deng, L. Zheng, Q. Ye, G. Kang, Y. Yang, and J. Jiao. Image-image domain adaptation with preserved self-similarity and domain-dissimilarity for person re-identification. *2018 IEEE/CVF Conference on Computer Vision and Pattern Recognition*, pages 994–1003, 2018.
- [8] Epic Games. Unreal engine 4. version 4.22.1, April 2019.
- [9] Z. F., L. S., X. GS., Z. J., Z. K., and S. L. Unsupervised domain adaptation with noise resistible mutual-training for person re-identification. *Computer Vision – ECCV 2020*, 2020.
- [10] Y. Ge, D. Chen, and H. Li. Mutual mean-teaching: Pseudo label refinery for unsupervised domain adaptation on person re-identification. *International Conference on Learning Representations*, 2020.
- [11] I. J. Goodfellow, J. Pouget-Abadie, M. Mirza, B. Xu, D. Warde-Farley, S. Ozair, A. Courville, and Y. Bengio. Generative adversarial networks. *NIPS'14: Proceedings of the 27th International Conference on Neural Information Processing Systems*, 2:2672–2680, December 2014.
- [12] D. Gray, S. Brennan, and H. Tao. Evaluating appearance models for recognition, reacquisition, and tracking. *Proc. IEEE international workshop on performance evaluation for tracking and surveillance (PETS)*, 3(5):1–7, 2007.
- [13] M. Guillaumin, J. Verbeek, and C. Schmid. Is that you? metric learning approaches for face identification. *2009 IEEE 12th International Conference on Computer Vision*, pages 498–505, 2009.
- [14] K. He, X. Zhang, S. Ren, and J. Sun. Deep residual learning for image recognition. *2016 IEEE Conference on Computer Vision and Pattern Recognition (CVPR)*, pages 770–778, 2016.
- [15] M. Hirzer, C. Beleznai, P. M. Roth, and H. Bischof. Person re-identification by descriptive and discriminative classification. *Proceedings of the 17th Scandinavian conference on Image analysis*, pages 91–102, May 2011.
- [16] S. Ioffe and C. Szegedy. Batch normalization: Accelerating deep network training by reducing internal covariate shift. *Proceedings of Machine Learning Research*, 37:448–456, July 2015.
- [17] S. karanam, M. Gou, Z. Wu, A. Rates-Borras, O. Camps, and R. J. Radke. Systematic evaluation and benchmark for person re-identification: Features, metrics, and datasets. *IEEE Transactions on Pattern Analysis and Machine Intelligence*, 41(3):523–536, 2018.
- [18] M. Koestinger, M. Hirzer, P. Wohlhart, P. M. Roth, and H. Bischof. Large scale metric learning from equivalence constraints. *2012 IEEE conference on computer vision and pattern recognition*, pages 2288–2295, June 2012.
- [19] A. Krizhevsky, I. Sutskever, and G. Hinton. Imagenet classification with deep convolutional neural networks. *Neural Information Processing Systems*, 25, January 2012.
- [20] W. Li, R. Zhao, and X. Wang. Human reidentification with transferred metric learning. *Asian conference on computer vision - ACCV 2012*, pages 31–44, 2012.
- [21] W. Li, R. Zhao, T. Xiao, and X. Wang. Deepreid: Deep filter pairing neural network for person re-identification. *2014 IEEE Conference on Computer Vision and Pattern Recognition*, pages 152–159, 2014.
- [22] S. Paisitkriangkrai, C. Shen, and A. van den Hengel. Learning to rank in person re-identification with metric ensembles. *2015 IEEE Conference on Computer Vision and Pattern Recognition (CVPR)*, pages 1846–1855, 2015.
- [23] P. Peng, T. Xiang, Y. Wang, M. Pontil, S. Gong, T. Huang, and Y. Tian. Unsupervised cross-dataset transfer learning for person re-identification. *2016 IEEE Conference on Computer Vision and Pattern Recognition (CVPR)*, pages 1306–1315, 2016.
- [24] E. Ristani, F. Solera, R. S. Zou, R. Cucchiara, and C. Tomasi. Performance measures and a data set for multi-target, multi-camera tracking.

Computer Vision – ECCV 2016 Workshops., 2016.

[25] H. E. Ross, E. D. J. Murray, and E. H. Weber. E. h. weber on the tactile senses (2nd ed.). *Erlbaum (Uk) Taylor & Francis, Publ.*, 1996.

[26] A. Shrivastava, T. Pfister, O. Tuzel, J. Susskind, W. Wang, and R. Webb. Learning from simulated and unsupervised images through adversarial training. *Proceedings of the IEEE conference on computer vision and pattern recognition*, pages 2107–2116, 2017.

[27] L. Song, C. Wang, L. Zhang, B. Du, Q. Zhang, C. Huang, and X. Wang. Unsupervised domain adaptive re-identification: Theory and practice. *Pattern Recognition*, 102(0031-3203):107173, 2020.

[28] N. Srivastava, G. Hinton, A. Krizhevsky, I. Sutskever, and R. Salakhutdinov. Dropout: A simple way to prevent neural networks from overfitting. *Journal of Machine Learning Research*, 15(56):1929–1958, 2014.

[29] X. Sun and L. Zheng. Dissecting person re-identification from the viewpoint of viewpoint. *2019 IEEE/CVF Conference on Computer Vision and Pattern Recognition (CVPR)*, pages 608–617, 2019.

[30] Y. Sun, L. Zheng, W. Deng, and S. Wang. Svdnet for pedestrian retrieval. *2017 IEEE International Conference on Computer Vision (ICCV)*, pages 3820–3828, 2017.

[31] Y. Sun, L. Zheng, Y. Yang, Q. Tian, and S. Wang. Beyond part models: Person retrieval with refined part pooling (and a strong convolutional baseline). *Proceedings of the European Conference on Computer Vision (ECCV)*, pages 501–518, September 2018.

[32] C. Szegedy, W. Liu, Y. Jia, P. Sermanet, S. Reed, D. Anguelov, D. Erhan, V. Vanhoucke, and A. Rabinovich. Going deeper with convolutions. *2015 IEEE Conference on Computer Vision and Pattern Recognition (CVPR)*, pages 1–9, 2015.

[33] G. Wang, Y. Yuan, X. Chen, J. Li, and X. Zhou. Learning discriminative features with multiple granularities for person re-identification. *Proceedings of the 26th ACM international conference on Multimedia*, pages 274–282, October 2018.

[34] J. Wang, X. Zhu, S. Gong, and W. Li. Transferable joint attribute-identity deep learning for unsupervised person re-identification. *2018 IEEE/CVF Conference on Computer Vision and Pattern Recognition*, pages 2275–2284, 2018.

[35] T. Wang, S. Gong, X. Zhu, and S. Wang. Person re-identification by video ranking. *Computer Vision – ECCV 2014*, 8692:688–703, 2014.

[36] L. Wei, S. Zhang, W. Gao, and Q. Tian. Person transfer gan to bridge domain gap for person re-identification. *2018 IEEE/CVF Conference on Computer Vision and Pattern Recognition*, pages 79–88, 2018.

[37] K. Q. Weinberger and L. K. Saul. Fast solvers and efficient implementations for distance metric learning. *Proceedings of the 25th international conference on Machine learning*, pages 1160–1167, July 2008.

[38] D. Wu, S.-J. Zheng, X.-P. Zhang, C.-A. Yuan, F. Cheng, Y. Zhao, Y.-J. Lin, Z.-Q. Zhao, Y.-L. Jiang, and D.-S. Huang. Deep learning-based methods for person re-identification: A comprehensive review. *Neurocomputing*, 337(14):354–371, April 2019.

[39] S. Xiang, Y. Fu, G. You, and T. Liu. Taking a closer look at synthesis: Fine-grained attribute analysis for person re-identification. *ICASSP 2021 - 2021 IEEE International Conference on Acoustics, Speech and Signal Processing (ICASSP)*, pages 3765–3769, 2021.

[40] T. Xiao, H. Li, W. Ouyang, and X. Wang. Learning deep feature representations with domain guided dropout for person re-identification. *Proceedings of the IEEE conference on computer vision and pattern recognition*, pages 1249–1258, 2016.

[41] M. Ye, X. Lan, and P. C. Yuen. Robust anchor embedding for unsupervised video person re-identification in the wild. *Proceedings of the European Conference on Computer Vision (ECCV)*, pages 170–186, 2018.

[42] M. Ye, J. Shen, G. Lin, T. Xiang, L. Shao, and S. C. Hoi. Deep learning for person re-identification: A survey and outlook. *IEEE Transactions on Pattern Analysis and Machine Intelligence*, 2021.

[43] H.-X. Yu, A. Wu, and W.-S. Zheng. Cross-view asymmetric metric learning for unsupervised person re-identification. *2017 IEEE International Conference on Computer Vision (ICCV)*, pages 994–1002, 2017.

[44] Y. Zhai, S. Lu, Q. Ye, X. Shan, J. Chen, R. Ji, and Y. Tian. Ad-cluster: Augmented discriminative clustering for domain adaptive person re-identification. *Proceedings of the IEEE/CVF Conference on Computer Vision and Pattern Recognition*, pages 9021–9030, 2020.

[45] Z. Zhang, C. Lan, W. Zeng, X. Jin, and Z. Chen. Relation-aware global attention for person re-identification. *Proceedings of the IEEE/CVF Conference on Computer Vision and Pattern Recognition*, pages 3186–3195, 2020.

[46] L. Zheng, L. Shen, L. Tian, S. Wang, J. Wang, and Q. Tian. Scalable person re-identification: A benchmark. *2015 IEEE International Conference on Computer Vision (ICCV)*, pages 1116–1124, 2015.

[47] L. Zheng, Y. Yang, and A. G. Hauptmann. Person re-identification: Past, present and future. *arXiv preprint arXiv:1610.02984*, 2016.

[48] Z. Zhong, L. Zheng, D. Cao, and S. Li. Re-ranking person re-identification with k-reciprocal encoding. *2017 IEEE Conference on Computer Vision and Pattern Recognition (CVPR)*, pages 3652–3661, 2017.

[49] Z. Zhong, L. Zheng, Z. Zheng, S. Li, and Y. Yang. Camstyle: A novel data augmentation method for person re-identification. *IEEE Transactions on Image Processing*, 28(3):1176–1190, March 2019.

[50] J.-Y. Zhu, T. Park, P. Isola, and A. A. Efros. Unpaired image-to-image translation using cycle-consistent adversarial networks. *Computer Vision (ICCV), 2017 IEEE International Conference on*, pages 2242–2251, 2017.

[51] Y. Zou, X. Yang, Z. Yu, B. Kumar, and J. Kautz. Joint disentangling and adaptation for cross-domain person re-identification. *Computer Vision – ECCV 2020*, 2020.